Talanta 228 (2021) 122213

Contents lists available at ScienceDirect

Talanta

journal homepage: www.elsevier.com/locate/talanta

A novel THz molecule-selective sensing strategy in aqueous environments: THz-ATR spectroscopy integrated with a smart hydrogel

Jie Zhou [a,1], Xuemei Wang [b,1], Yunxia Wang [a], Guorong Huang [a], Xiang Yang [a], Yang Zhang [a], Yu Xiong [a], Lu Liu [a], Xiang Zhao [c,**], Weiling Fu [a,*]

[a] Department of Laboratory Medicine, Southwest Hospital, Third Military Medical University (Army Medical University), Chongqing, 400038, China
[b] Department of Laboratory Medicine, Daping Hospital, Third Military Medical University (Army Medical University), Chongqing, 400042, China
[c] Department of Oncology, Southwest Hospital, Third Military Medical University (Army Medical University), Chongqing, 400038, China

ARTICLE INFO

Keywords:
Terahertz spectroscopy
Smart hydrogel
Selective detection
Biosensor

ABSTRACT

Terahertz (THz) spectroscopy, with fascinating advantages for biomedical applications, is still in its infancy in terms of the selective detection of aqueous biomolecules because the strong absorption of solvent water always obscures the THz spectroscopic features of biomolecules. Nevertheless, solvent water is not a passive spectator but a useful indicator, as this proposed strategy describes. This strategy utilizes THz attenuated total reflection (THz-ATR) spectroscopy to probe the glucose-induced hydration state changes of smart hydrogels for label-free and selective detection of aqueous glucose. A notable dramatic increase in both the THz absorption coefficient and hydration state (calculated by weighing) of the smart hydrogel was observed with increasing aqueous glucose concentration, which was further verified by a simple two-component model. For aqueous glucose sensing, this method surpasses individual THz-ATR devices and exhibits suitable sensitivity, ideal selectivity and excellent reusability. Moreover, the proposed strategy may provide an alternative option for the selective detection of various aqueous molecules by THz spectroscopy.

1. Introduction

Terahertz (THz) spectroscopy, as an emerging label-free and nonionizing detection technology, could unravel the mystery of long-range and intermolecular vibrational modes and is especially adaptable for probing the function, conformation, and hydration dynamics of biomolecules. Owing to the abundant distinct features in THz absorption spectra, many molecules comprising carbohydrates, amino acids, nucleotides [1] and methylated DNA [2] can be precisely identified in their dry or frozen state, referred to as THz spectral fingerprint identification. With regard to THz biosensing in aqueous environments, the biomolecule-induced hydration dynamics can also be monitored by THz absorption spectroscopy on the sub-picosecond time scale [3]. Consequently, with distinct water-sensitive properties, THz absorption spectroscopy has been used to distinguish tumour cells from normal cells, identify bacterial species and viability and observe dehydration dynamics in biological tissues based on hydration state differences [4,5].

However, aqueous molecules exhibit only a concentration-dependent increase or decrease in THz absorption with scarcely any characteristic spectroscopic features; the identification of aqueous molecules in the THz range cannot depend on their features that exist in the solid state because of the strong THz absorption by liquid water (~240 cm^{-1} @ 1 THz) [1]. For instance, in aqueous glucose, the THz absorption induced by the collective intermolecular vibrations of the hydrogen bond water network far surpasses that of glucose, thus obscuring the clear absorption peak (@ 1.4 THz) belonging to solid-state glucose [6]. Moreover, overcoming the current limitation, in which the commonly transmitted THz signal is severely attenuated by aqueous environments, has been ongoing, involving many feasible proposed strategies, such as the use of THz attenuated total reflection (THz-ATR) [7], metamaterials [8], microfluidics [9] and optical clearing agents [10]. As listed in Table S1, these strategies can be divided into two categories: enhancing the interaction between THz waves and aqueous samples via evanescent waves (THz-ATR) and spoof surface plasmons

* Corresponding author.
** Corresponding author.
E-mail addresses: x.zhao.tmmu@outlook.com (X. Zhao), weiling_fu@126.com (W. Fu).
[1] These authors contributed equally.

https://doi.org/10.1016/j.talanta.2021.122213
Received 14 October 2020; Received in revised form 7 February 2021; Accepted 10 February 2021
Available online 16 February 2021

(metamaterials) and weakening the attenuation of aqueous samples by reducing the test volume (microfluidics) and replacing highly absorptive water molecules (optical clearing agents). Although the detection selectivity of THz spectroscopy, recognizing different aqueous biomolecules, has been partly promoted by antibody-antigen [11] or aptamer-target binding reactions [12] and conjugated avidin-AuNPs [13], this technique is still in its infancy and has difficulty satisfying the clinical requirements.

A smart hydrogel is a highly hydrophilic crosslinked polymer forming a three-dimensional (3D) network that can respond properly to adequate external stimuli, exhibiting intelligent swelling-shrinking behavior and hydration state variation [14]. Due to the high biorecognition efficiency of the 3D network, the target-induced recognition event of a smart hydrogel can be transformed into detectable signals, which has the advantages of a large surface-area-to-volume ratio, high biocompatibility, functional versatility and mechanical stability. To date, various smart hydrogels have been designed to detect small molecules [15], proteins [16], nucleic acids [17] and even viruses [18]. In particular, based on the increasing number of hydrophilic species in the hydrogel network caused by reversible ester binding reactions between boronic acid and diol groups, smart hydrogels decorated with 3-acrylamidophenylboronic acid (AAPBA) could reversibly bind to saccharides, including glucose and polyols, and usually experience profound hydration state changes. Smart hydrogels bearing AAPBA are also called "glucose-responsive" smart hydrogels. Hence, considering the target-responsive hydration state shift of a smart hydrogel and the strong water absorption in the THz range, speculating that integrating THz spectroscopy with a smart hydrogel may generate the unique advantage of selectively detecting aqueous glucose is reasonable. More importantly, different from the above methods that rarely use or even remove water molecules, this assumption treats water molecules as sensing indicators, thus possibly providing a novel THz molecule-selective sensing strategy for aqueous environments.

Inspired by previous studies, we developed a strategy in which we first attempt to introduce a smart hydrogel into a THz-ATR device for the selective and label-free detection of aqueous glucose. The smart hydrogel sheet was made through an ultraviolet (UV) gel curing process in a homemade mould, and the mass fraction of AAPBA was optimized by a weighing method. Then, the THz absorption spectra of smart hydrogels, achieving swelling equilibrium in aqueous glucose of various concentrations, were obtained and compared with that of separate aqueous glucose, preliminarily demonstrating the superiority of this joint method. Moreover, we used the weighing method and two-component model to analyze the origin of the THz absorption difference of the reacted smart hydrogel. Finally, the sensing performance of the proposed method was also investigated, showing promising potential for clinical applications.

2. Material and methods

2.1. Materials

Glucose-responsive smart hydrogels were prepared using 2-hydroxyethyl methacrylate (HEMA) as the main-chain monomer, ethylene glycol dimethacrylate (EGDM) as the crosslinker, 2,2-dimethoxy-2-phenylacetophenone (DMPA) as the photoinitiator and AAPBA as the recognized element. The buffer solution was made by mixing 2-(cyclohexylamino)ethanesulfonic acid (CHES, Solarbio Science & Technology Co., Ltd., China) and sodium chloride. Through monitoring with a pH meter (FiveGo F2, Mettler-Toledo International Inc., USA), the pH was adjusted to 9.0 and 7.4 with 1 M sodium hydroxide solution. Then, this solution was used to prepare glucose, fructose, galactose and sodium lactate solutions of different concentrations. To mimic real sample analysis, bovine serum albumin (BSA) with a final concentration of 3 g/L was added into different aqueous glucose solutions (20 mg/dL, 80 mg/dL and 200 mg/dL). All reagents were obtained from Sigma-Aldrich unless otherwise noted, and all solutions were made from ultrapure water (Milli-Q, Millipore, 18.2 MΩ.cm resistivity).

2.2. Synthesis of smart hydrogel sheets

The precursor solution was prepared by dissolving AAPBA (45 mg), DMPA (18 mg) and EGDM (7 mg) in HEMA (430 mg) and then mixing them in a microcentrifuge tube after it was wrapped by aluminium foil, similar to previous research [19]. Then, the mixture after being shaken vigorously was added into a Teflon mould and irradiated under a UV lamp (λ = 365 nm) for 15 min. Therewith, it was incubated in CHES buffer overnight to remove the unpolymerized monomers and gently peeled from the Teflon mould by tweezers, and swelling equilibrium was then realized by replacing the buffer solution every 6 h.

2.3. Weighing measurement of the reacted smart hydrogel

To evaluate the swelling ratio of the smart hydrogel in aqueous glucose of different concentrations, we first investigated the reaction kinetics of the smart hydrogel and found that the absorption coefficients were saturated 28 h after the reaction began (SI, Fig. S1). Then, the hydrogel was incubated in the corresponding aqueous glucose with replacement every 6 h for two days until completely reaching the swelling equilibrium. The remaining buffer droplets on the hydrogel sheet were completely removed by dust-free paper (Kimberly-Clark Worldwide, Inc., USA), and its weight was quickly obtained by an analytical balance (XB124, Precisa, Switzerland). Subsequently, the normalized signal variation ΔS of the weight or THz absorption coefficient of the smart hydrogel was calculated using Eq. (1):

$$\Delta S = \left|\frac{S_c - S_0}{S_0}\right|, \tag{1}$$

where S_0 and S_c refer to the measured weight or THz absorption coefficient values after swelling equilibrium in the CHES buffer and the corresponding aqueous glucose, respectively.

2.4. THz measurement of the glucose pellet and smart hydrogel

Glucose pellets were made by glucose powder to prepare the 0.80 mm-thick pellets compressed by a pressure of 10 MPa for 2 min. The THz spectra of glucose pellets were measured by a THz time-domain spectroscopy system in transmission mode (TAS 7500SP, Advantest Co., Japan). The THz response of the reacted smart hydrogel was obtained in ATR mode. Based on previous studies [20] and calculation results (SI, Fig. S2), the penetration depth (approximately tens of micrometres @ 0.4–2.0 THz) of the evanescent waves was much smaller than the thickness of the smart hydrogel sheet (approximately 1 mm), so we can use the "prism-hydrogel" model to obtain the THz absorption coefficient of the smart hydrogel [21]. Specifically, we calculated Fresnel's reflection coefficient ($\tilde{r}_{12}$) of the prism-hydrogel interface by the reflectance ($\tilde{R}$) and phase spectrum ($\tilde{\phi}$), which were obtained from the THz time-domain spectrum after Fourier transform, as shown in Eqs. (2) and (3):

$$\tilde{R} = \left|\frac{\tilde{r}_{12}}{r_{REF}}\right|^2 \tag{2}$$

$$\tilde{\phi} = Arg\left[\frac{\tilde{r}_{12}}{r_{REF}}\right] \tag{3}$$

where r_{REF} refers to the reflection coefficient of the prism-air interface (reference signal). $\tilde{r}_{12}$ can also be calculated as a function of the THz wave incident angle (θ) and the complex permittivities of the ATR prism (ε_1) and hydrogel ($\tilde{\varepsilon}_2$). The complex permittivity of the hydrogel sheet can be obtained with determination of other parameters, as shown in Eq. (4):

$$\tilde{r}_{12} = \frac{\sqrt{\varepsilon_1}\sqrt{1-(\frac{\varepsilon_1}{\tilde{\varepsilon}_2})\sin^2\theta} - \sqrt{\tilde{\varepsilon}_2}\cos\theta}{\sqrt{\varepsilon_1}\sqrt{1-(\frac{\varepsilon_1}{\tilde{\varepsilon}_2})\sin^2\theta} + \sqrt{\tilde{\varepsilon}_2}\cos\theta} \quad (4)$$

The relationship between the extinction coefficient (κ) and refractive index (n) of the hydrogel and the imaginary part (ε'') and real part (ε') of the complex permittivity ($\tilde{\varepsilon}_2$) of the hydrogel are given by Eqs. (5) and (6):

$$\varepsilon' = n^2 - \kappa^2 \quad (5)$$

$$\varepsilon'' = 2n\kappa \quad (6)$$

Then, the absorption coefficient (α) of the hydrogel can be calculated according to the extinction coefficient, angular frequency (ω) and speed of light (c) as in Eq. (7).

$$\alpha = \frac{2\omega\kappa}{c} \quad (7)$$

The reacted smart hydrogel sheet was quickly weighed by an electronic balance and then measured by a THz-ATR device, in which the sheet was pressed closely onto the surface of the THz-ATR prism with uniform and appropriate pressure by a pressure clamp. The bare prism was used as the reference signal. All the above measurements were carried out three times under an ambient temperature of 26 ± 0.5 °C and a humidity of less than 5%.

3. Results and discussion

3.1. Principle of the proposed method

For sensing aqueous biological samples in the THz range, we introduce the smart hydrogel as a sensing medium whose hydration state is highly sensitive to shifts in aqueous glucose. A scheme of the working components of the sensing device is shown in Fig. 1a, which consists of a THz-ATR prism and a glucose-responsive smart hydrogel. In the THz-ATR device, the incident THz wave is propelled to the upper interface of the THz-ATR prism and then generates evanescent waves that penetrate the sample attached to the surface of the prism and distribute up to tens of micrometres thick. Due to this strong interaction between the evanescent waves and sample, the output THz wave contained the permittivity parameters of the sample; thus, the complex permittivity of attached samples can be obtained with the above "prism-hydrogel" model [22]. Namely, compared with transmission or reflection mode, THz-ATR spectroscopy is very suitable for highly absorptive samples regardless of their morphology or volume and has been used to characterize various aqueous samples, such as aqueous protein, living cell monolayers, and microorganisms, and it may be especially suitable for evaluating the hydration state of smart hydrogels [7].

As a common recognition moiety decorated on the glucose-responsive smart hydrogel, AAPBA can be divided into two distinct

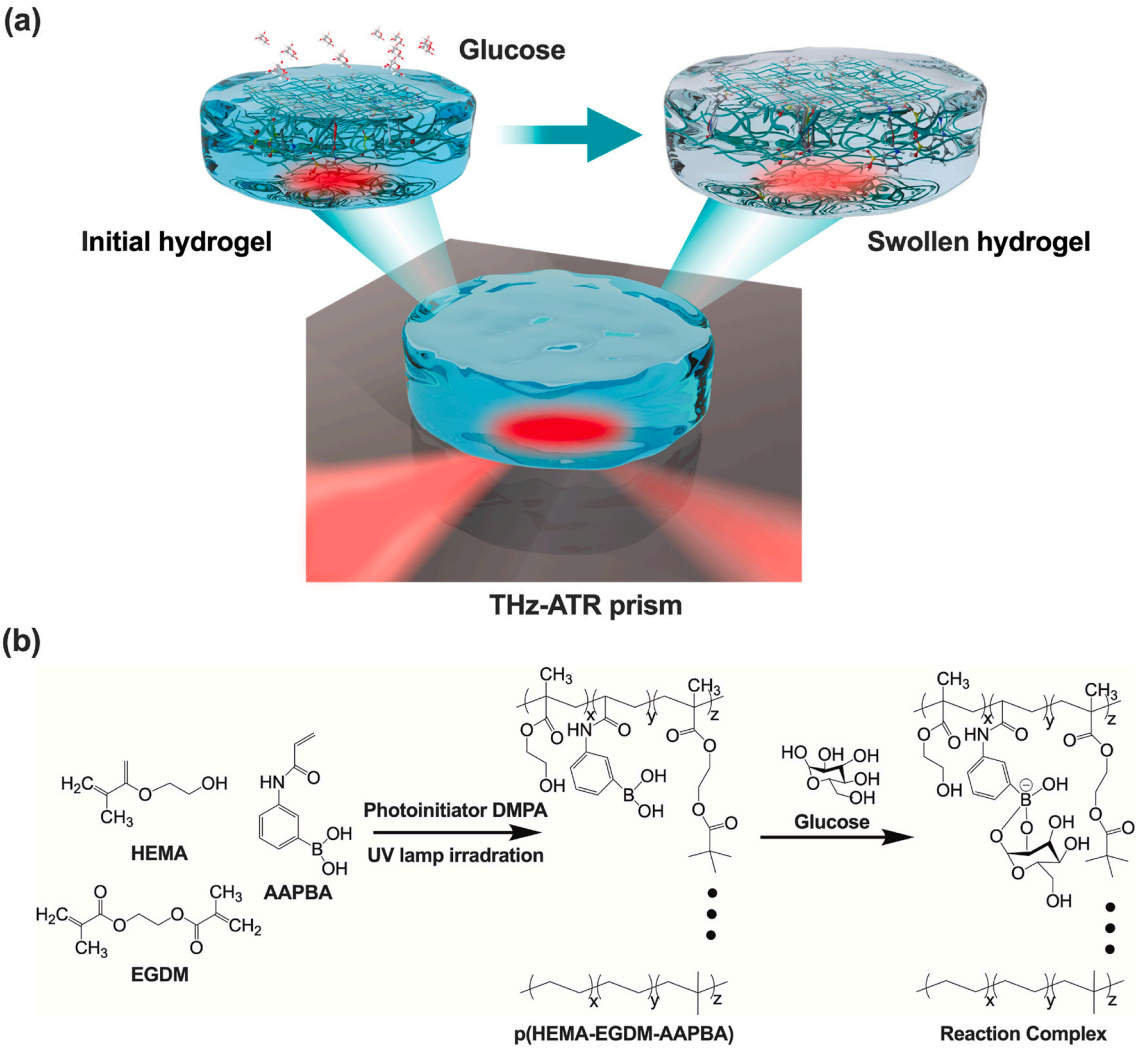

Fig. 1. (a) Schematic of THz-ATR spectroscopy integrated with a smart hydrogel. (b) Chemical structures of the precursor and the synthesis and reaction processes of the p(HEMA-EGDM-AAPBA) smart hydrogel.

forms at equilibrium in aqueous solutions: the neutral form (relatively hydrophobic) and charged form (relatively hydrophilic) [23]. The charged form can reversibly bind to aqueous glucose molecules with strong affinity to form a more stable charged 1:1 complex, leading to augmentation of the Donnan potential and hydrophilic substances in the polymerized hydrogel network (Fig. 1b), thus altering the volume and hydration state of the smart hydrogel. Since the formation and breaking of the hydrogen bond network of bulk water molecules occur on the picosecond time scale, THz absorption spectroscopy directly probes the tiny variations in the collective hydrogen bond network dynamics of the polymer and thereby assesses its hydration state change [3]. Specifically, the THz absorption would rise with increasing hydration state, according to previous study [24]. As a result, the hydration shift of the smart hydrogel induced by glucose may bring about remarkable changes in THz absorption, which could be used for molecule-selective sensing in aqueous environments.

3.2. Feasibility of the proposed strategy

As expected, more AAPBA molecules could bring about a more profound hydration state change of the smart hydrogel, while the solubility of AAPBA should also be considered [25]. We determined the optimal mass fraction of AAPBA in the precursor solution to be 9 wt% (SI, Fig. S3a and S3b), with which the hydrogel possesses an appropriate uniformity and a better glucose responsiveness. The reaction temperature and pH were also investigated (SI, Fig. S3c), which demonstrated that the smart hydrogel would experience more profound signal change at room temperature (~26 °C) and pH 9.0. Then, THz-ATR absorption spectroscopy was utilized to acquire the absorption changes corresponding to variations in the hydration state of the smart hydrogel caused by aqueous glucose under the optimized condition. As shown in Fig. 2a, aqueous glucose loses its characteristic spectroscopic feature at 1.44 THz that exists in its solid state (red dotted line), only exhibiting a flat and featureless curve similar to that of other aqueous molecules. With regard to the smart hydrogel, its measured absorption coefficient is lower than that of aqueous glucose. Interestingly, the smart hydrogel demonstrates a significantly increased absorption intensity after incubation in a physiological concentration (80 mg/dL) of aqueous glucose, while a change in the aqueous glucose concentration (0 mg/dL versus 80 mg/dL) has no effect on the THz absorption curve.

Fig. 2b and c further validates the concentration dependence of the THz absorption curves of the smart hydrogel and the corresponding aqueous glucose. The absorption coefficient of the smart hydrogel gradually increases with increasing THz frequency and displays an increasing trend with significant differences when incubated in aqueous glucose of various concentrations (0, 20, 40, 80, 100, 200, and 300 mg/dL). The normalized variation in the absorption coefficients (@ 1 THz) of the reacted smart hydrogel is calculated by Eq. (1). Clearly, the normalized signal variation for the smart hydrogel (red solid line) increases as the aqueous glucose concentration increases (Fig. 2d) in contrast to the slightly normalized signal variation observed for aqueous glucose (black solid line), whose error bars partially overlap in the THz absorption curve. The proposed sensing method, integrating a THz-ATR device with a target-responsive smart hydrogel, seems feasible for the

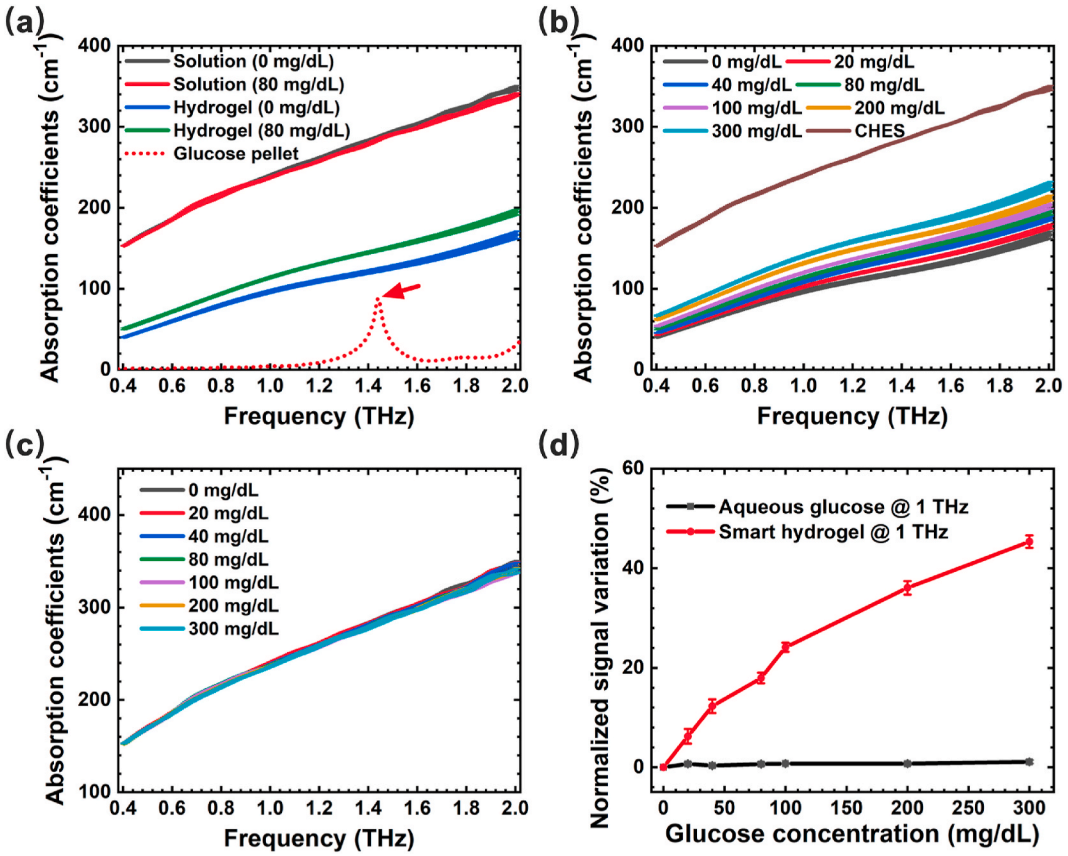

Fig. 2. (a) Comparison of the absorption spectra of the glucose pellet, aqueous glucose (0 mg/dL versus 80 mg/dL) and smart hydrogels before and after reaching swelling equilibrium in aqueous glucose (80 mg/dL). Red arrow points to the unique THz absorption peak of the glucose pellet at 1.44 THz, which disappears in aqueous glucose. (b) Absorption spectra of CHES buffer and smart hydrogels after reaching swelling equilibrium in aqueous glucose with different concentrations. (c) Absorption spectra of aqueous glucose with different concentrations. (d) Comparison of the normalized variations in the absorption coefficient of the smart hydrogel after reaching swelling equilibrium in different aqueous glucose solutions and of separate aqueous glucose at 1 THz. Error bars indicate the standard deviation (N = 3). (For interpretation of the references to colour in this figure legend, the reader is referred to the Web version of this article.)

selective detection of aqueous samples.

The phenomenon that the THz absorption curve of the reacted smart hydrogel gradually approaches that of the CHES buffer as the aqueous glucose concentration increases suggests that the smart hydrogel may experience significant hydration state changes, which is also verified by the significant weight variation during the optimization of the precursor solution. In contrast, the THz absorption curves for various aqueous glucose solutions are indistinguishable, except for the slight decrease for the 300 mg/dL aqueous glucose, which may stem from the effects of water replacement. Furthermore, for the 200 mg/dL concentration, the normalized absorption variation of the smart hydrogel (~36.08%) is approximately 50 times that of the separate aqueous glucose (~0.72%), exhibiting a much better signal enhancement effect. This effect comes from the unique enrichment of glucose molecules by the smart hydrogel through selective PBA-diol binding reactions, which generate corresponding hydration state changes in the hydrogel network. However, the 300 mg/dL concentration, the maximum concentration in the measurement, refers to a mass fraction of 0.3% for glucose molecules in aqueous environments; thus only a slight "THz defect" or "THz excess" effect may occur, which results in the partially overlapping THz absorption curves obtained by the individual THz-ATR device. Therefore, benefiting from the target-responsive smart hydrogel, the THz-ATR device can clearly identify the signal variance of aqueous glucose within the physiological concentration range, which has hardly been achieved before.

3.3. Origins of the hydrogel absorption variation

The weighing method was carried out to further investigate the origin of the difference in the THz absorption curve of the reacted smart hydrogel [26]. Utilizing this widely used method, the hydration state change of the smart hydrogel could be calculated by comparing the weight before and after swelling in aqueous glucose. Given that the apparent binding equilibrium constant between phenylboronic acid and glucose was estimated to be 12.5 M^{-1} and the mass fraction of AAPBA in the precursor solution was only 9% [27], the normalized weight change of the swollen smart hydrogel sheet at a concentration of 300 mg/dL (~16.67 mM) is mainly derived from additional water rather than from bound glucose. Accordingly, the normalized weight variation of the smart hydrogel well matches its normalized absorption variation as the glucose concentration increases, and their linear correlation is strong ($R^2 = 0.99443$), as shown in Fig. 3a.

Moreover, a useful two-component model, $\alpha_{prediction} = \alpha_0 \times \frac{W_0}{W_c} + \alpha_{CHES} \times (\frac{W_c - W_0}{W_c})$, was proposed to analyze the contribution of the hydration state change [28], where W_0 and W_c are the weights of the smart hydrogel before and after swelling, and α_o, $\alpha_{prediction}$ and α_{CHES} are the initial and predicted absorption coefficients of the swollen smart hydrogel and that of the CHES buffer, respectively. This model is based on the assumption that the augmentation of the hydration state of the reacted smart hydrogel mainly results in a corresponding change in its absorption coefficient. As illustrated in Fig. 3b, the predicted and measured curves of the smart hydrogel after incubation are almost the same, especially in the frequency range of 0.8 THz to 2.0 THz. These trends, that a hydration state change brings about a profound absorption variation, are in good agreement with previous study [24]. Namely, the increasing hydration state and the relatively high difference in the absorption coefficients of the initial smart hydrogel and water could yield a much more pronounced variation in the measured THz absorption spectra. Therefore, we deem that the absorption changes of the reacted smart hydrogel indeed originate from the shift of its hydration state response to aqueous glucose. This further supports the rationality of the proposed design and provides a basic principle for the selective detection of aqueous targets by THz absorption spectroscopy. Additionally, this THz-based method, complementary to other characterization techniques, directly probes the complete details of hydration dynamics changes in the smart hydrogel network in a label-free manner.

3.4. Sensing performance of the proposed strategy

The sensing performance of this proposed analytical device was evaluated, including the sensitivity, selectivity, reusability and stability. Fig. 4a shows that within the glucose concentration range (0–200 mg/dL), with a clinical diagnostic value, the absorption coefficient of the smart hydrogel gradually saturates with increasing glucose concentration. The analytical device presents a linear response for a glucose concentration range of 0–200 mg/dL with correlation coefficient $R^2 = 0.96108$, and the limit of detection is 17.72 mg/dL (Signal to noise ratio of 3), which is basically identical to that in reported study [29]. Given the complexity of the biological sample composition, the molecules bearing cis-diols and α-hydroxy acids and other polyols (free glycerol, catecholamine, *etc*.) would interact with AAPBA in the same way as glucose. To explore the selectivity of the smart hydrogel to common interferents in human blood, fructose, galactose, and lactate were selected due to their relatively high physiological concentration. The calculation of the degree of interference (DI) from interfering substances referred to the formula $DI = \frac{\alpha_I - \alpha_{80}}{\alpha_{80} - \alpha_0}$, where α_0, α_I and α_{80} represent the

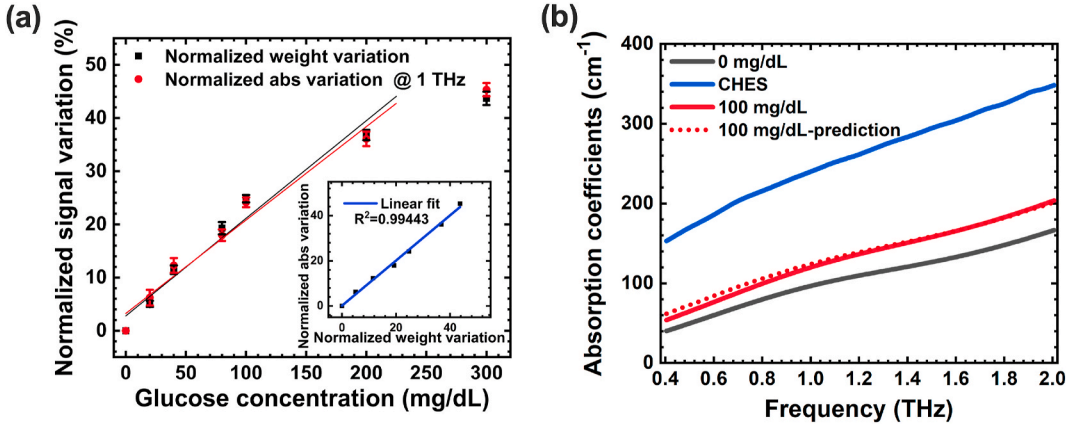

Fig. 3. (a) Normalized variation in the absorption coefficient at 1 THz and weight of the smart hydrogel in aqueous glucose with different concentrations and their fitting results. (Inset) Fitting result of the normalized change of the weight and absorption coefficient at 1 THz of the smart hydrogel. (b) Comparison between the predicted absorption curves (red dotted line) of the smart hydrogel at 100 mg/dL aqueous glucose based on the two-component model and the measured absorption curves of CHES buffer (blue solid line) and the smart hydrogel at 0 mg/dL (black solid line) and 100 mg/dL (red solid line) aqueous glucose. Error bars indicate the standard deviation (N = 3). (For interpretation of the references to colour in this figure legend, the reader is referred to the Web version of this article.)

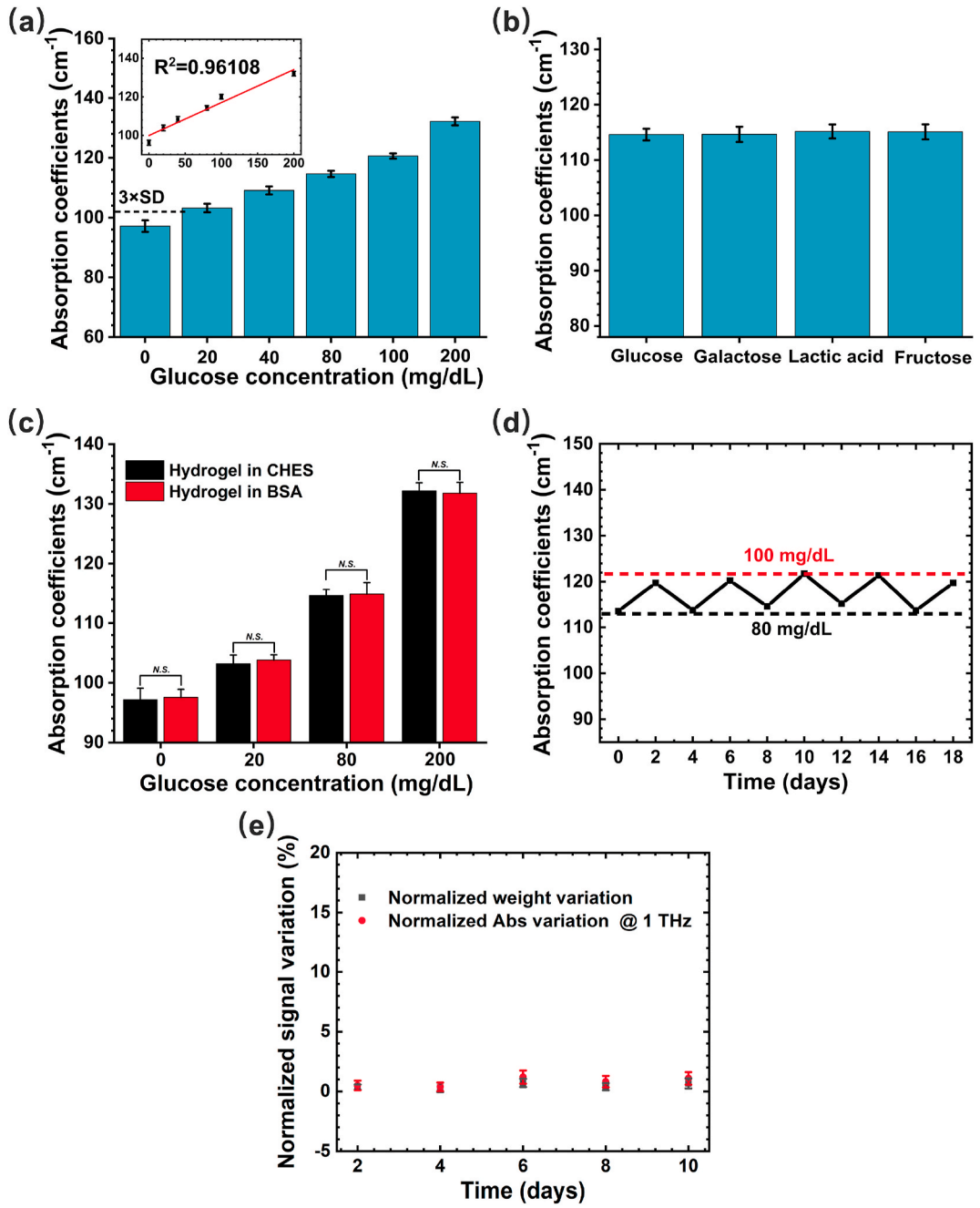

Fig. 4. (a) Sensitivity evaluation of the THz-ATR platform integrated with a smart hydrogel for the detection of aqueous glucose. (Inset) Fitting result between the absorption coefficient of the smart hydrogel in aqueous glucose with different concentrations after reaching swelling equilibrium and the corresponding aqueous glucose concentration. (b) Interference evaluation, from left to right: 80 mg/dL aqueous glucose, 80 mg/dL aqueous glucose containing 2 mg/dL galactose, 80 mg/dL aqueous glucose containing 12 mg/dL lactic acid and 80 mg/dL aqueous glucose containing 2 mg/dL fructose. (c) Artificial real sample assay (pure aqueous glucose solutions containing 3 g/L BSA). *N.S.* represents no significant difference. (d) Reusability evaluation, continuous measurement of the absorption coefficient of the smart hydrogel after repeatedly reaching swelling equilibrium in 80 mg/dL and 100 mg/dL aqueous glucose. (e) Normalized change of the weight and absorption coefficient of the smart hydrogel in the CHES buffer at different times. The absorption coefficients in the Y-axis represent their values at 1 THz. Error bars indicate the standard deviation (N = 3).

absorption coefficient of the hydrogel after incubation in CHES buffer and in aqueous glucose (80 mg/dL) with or without interferents, respectively. As shown in Fig. 4b, no significant difference is observed in the absorption coefficient of the smart hydrogel after incubation in the separate aqueous glucose, and aqueous glucose solutions containing galactose (2 mg/dL), fructose (2 mg/dL) and lactic acid (12 mg/dL), respectively. The DIs are less than 5% (1.9%, 4.5%, and 4.9%). As with the literature precedent [27], although the affinity of fructose, galactose and lactic acid to AAPBA is higher than that of glucose, the proposed strategy was considered appropriately selective for aqueous glucose measurement since the primary interferents in human blood are present at much lower concentrations than glucose [30]. Furthermore, the interference of proteins in real sample analysis cannot be neglected. Recovery assays were utilized to investigate this interference by using the artificial real sample made of 3 g/L BSA and aqueous glucose at various concentrations. As shown in Fig. 4c, the absorption coefficients of the reacted smart hydrogel demonstrated no significant difference ($P > 0.05$) after incubation in pure aqueous glucose solutions and artificial

real samples. The recovery of glucose (ranging from 93.11% to 109.02%), with a relative standard deviation less than 5% (0.85%–1.71%), is listed in Table 1. This favourable ability of anti-protein interference was due to the hydroxyl groups and molecular sieve effect of the smart hydrogel network that could prevent protein absorption, which further proved that this strategy may have the potential to be applied for the quantitative detection of glucose in clinical samples.

Furthermore, the reusability of the smart hydrogel was investigated by recording the response process. The smart hydrogel displays little absorption drift or hysteresis when undergoing the repeated reaction process between aqueous glucose concentrations of 80 mg/dL and 100 mg/dL in 5 complete cycles (shown in Fig. 4d). The relative standard deviations are 0.62% and 0.79%. This proves that the smart hydrogel has highly reversible swelling-shrinking behavior and long-term stability of the readout signal responsiveness. In comparison to the drawbacks of the common glucose oxidase-based method, i.e., large signal drifts over time and immunological rejection [23], smart hydrogels reveal a more applicable sensing strategy with good biocompatibility and reusability for detecting aqueous targets in a real-time and label-free manner. Finally, we investigated the stability of the smart hydrogel. Fig. 4e shows that the weight and absorption coefficient of the hydrogel incubated in the CHES buffer did not change significantly during the observation period up to 10 days. This result emphasizes the satisfactory stability profiting from the fully chemically synthesized system and further confirms that the cause of the absorption variation is indeed the glucose-induced hydration state shift. Meaningfully, it also confirms the saturated swelling degree of the smart hydrogel under test despite the long swelling time.

The strong absorption of liquid water in the THz range will obscure any distinct biomolecular absorption peaks in the aqueous state, thus limiting numerous developed THz fingerprint-based selective sensing methods [9]. Benefiting from the unique hydration-state-change property of the target-responsive smart hydrogel, the proposed method can solve this problem, successfully transforming the selective detection of aqueous targets into a sensitive evaluation of hydration state changes by THz-ATR spectroscopy. That is, this method makes the best use of the advantages of THz-ATR spectroscopy and bypasses its disadvantages. Additionally, it seems to be versatile for multiple targets through the introduction of recognition elements such as aptamers or antibodies into the smart hydrogel network, which would be a valuable future research topic. Different from the reported methods that rely on sample exsiccation and optical cleaning agents to eliminate strong water absorption and improve the detection specificity, the proposed design could realize real aqueous sensing in the THz range without any unnecessary damage to the samples. In particular, the label-free and enzyme-free manner of this method provides the possibility of significantly reducing the operating environment dependence and test cost, revealing a competitive advantage in point-of-care applications.

The thickness of the smart hydrogel (approximately 1 mm) certainly exceeds the penetration depth of the evanescent waves, thus guaranteeing the reliability of the calculation model. Nonetheless, it greatly prolongs the swelling time of the smart hydrogel in aqueous glucose. The swelling time of the smart hydrogel is mainly affected by its crosslink density and thickness, the glucose concentration and the reaction temperature [29,31]. In this case, the time to reach complete swelling equilibrium was estimated to be close to 2 days for 20 mg/dL aqueous glucose at room temperature. In general, thin and low-density hydrogels lead to an ultrafast glucose response. Therefore, an ultrathin smart hydrogel-functionalized THz metamaterial is expected to achieve the fast and highly sensitive detection of aqueous glucose in the future.

In addition, since the binding of AAPBA to glucose is governed by the pKa of AAPBA and the pH of the solution, AAPBA shows high affinity to glucose molecules under the condition of pH $\geq$ its pKa. Therefore, this design is suitable for operation under high pH (e.g., pH = 9.0) conditions, but the performance at physiological pH is difficult to be satisfied. The sensor may be operated under physiological conditions and achieve high glucose selectivity by modifying the electron-withdrawing group on the aryl ring of phenylboronic acid (e.g., DDOPBA) or by introducing an electron-donating group (e.g., ATMA) into the smart hydrogel to decrease the pKa of phenylboronic acid [23]. Although the proposed strategy needs to be greatly improved, this state-of-the-art strategy is promising for the label-free, real-time and selective monitoring of aqueous biological samples in physiological environments, inspiring us to perfect the booming THz biosensing technology.

Table 1
Actual and measured concentration of glucose in artificial real samples (n = 3).

Added (mg/dL)	Measured (mg/dL)	RSD (%)	Recovery (%)
20	21.62	0.85	108.10
80	87.22	1.71	109.02
200	186.21	1.36	93.11

RSD: Relative standard deviation.

4. Conclusions

Aiming at the scarce selectivity of THz spectroscopy for aqueous biological sample detection, the proposed strategy complements the target-induced hydration state changes of a smart hydrogel with the strong water absorption in the THz range, whose feasibility was verified and explained by weighing and a two-component model. By integration of the smart hydrogel, the THz-ATR device could quantitatively and selectively detect aqueous glucose with moderate sensitivity, excellent reusability and ideal stability, which cannot be realized by separate THz spectroscopy. This sensing strategy offers the possibility to develop various smart hydrogel-functionalized THz sensing platforms by introducing aptamers, antibodies and enzymes into the hydrogel network. Future studies will concentrate on investigating the distinct THz absorption changes in the target-responsive "sol-gel" transition process of a DNA hydrogel and integrating this hydrogel into an ultrasensitive THz metamaterial for molecule-selective analysis in aqueous environments.

Funding

This work was supported by the Military Logistics Scientific Research Project (AWS17J010), the National Natural Science Foundation of China (82002250) and the Basic Science and Frontier Technology Research Project of Chong Qing (cstc2017jcyjBX0004).

Credit author statement

Jie Zhou: Conceptualization, Methodology, Investigation, Writing - Original Draft. Xuemei Wang: Investigation, Validation, Formal analysis. Yunxia Wang: Writing-Review & Editing, Funding acquisition. Guorong Huang: Project administration, Resources. Xiang Yang: Methodology, Data Curation. Yang Zhang: Visualization, Writing-Review & Editing. Yu Xiong: Resources, Visualization. Lu Liu: Resources, Visualization. Xiang Zhao: Conceptualization, Methodology, Writing - Review & Editing, Funding acquisition. Weiling Fu: Writing - Review & Editing, Supervision, Funding acquisition.

Declaration of competing interest

The authors declare that they have no known competing financial interests or personal relationships that could have appeared to influence the work reported in this paper.

Appendix A. Supplementary data

Supplementary data to this article can be found online at https://doi.org/10.1016/j.talanta.2021.122213.

References

[1] X. Yang, X. Zhao, K. Yang, Y. Liu, Y. Liu, W. Fu, Y. Luo, Biomedical applications of terahertz spectroscopy and imaging, Trends Biotechnol. 34 (2016) 810–824, https://doi.org/10.1016/j.tibtech.2016.04.008.

[2] H. Cheon, H.J. Yang, S.H. Lee, Y.A. Kim, J.H. Son, Terahertz molecular resonance of cancer DNA, Sci. Rep. 6 (2016) 37103, https://doi.org/10.1038/srep37103.

[3] V. Conti Nibali, M. Havenith, New insights into the role of water in biological function: studying solvated biomolecules using terahertz absorption spectroscopy in conjunction with molecular dynamics simulations, J. Am. Chem. Soc. 136 (2014) 12800–12807, https://doi.org/10.1021/ja504441h.

[4] Y. Wang, Z. Jiang, D. Xu, T. Chen, B. Chen, S. Wang, N. Mu, H. Feng, J. Yao, Study of the dielectric characteristics of living glial-like cells using terahertz ATR spectroscopy, Biomed. Optic Express 10 (2019) 5351–5361, https://doi.org/10.1364/BOE.10.005351.

[5] X. Yang, J. Shi, Y. Wang, K. Yang, X. Zhao, G. Wang, D. Xu, Y. Wang, J. Yao, W. Fu, Label-free bacterial colony detection and viability assessment by continuous-wave terahertz transmission imaging, J. Biophot. 11 (2018), e201700386, https://doi.org/10.1002/jbio.201700386.

[6] D.K. Lee, J.H. Kang, J.S. Lee, H.S. Kim, C. Kim, J. Hun Kim, T. Lee, J.H. Son, Q. H. Park, M. Seo, Highly sensitive and selective sugar detection by terahertz nano-antennas, Sci. Rep. 5 (2015) 15459, https://doi.org/10.1038/srep15459.

[7] K. Shiraga, T. Suzuki, N. Kondo, K. Tanaka, Y. Ogawa, Hydration state inside hela cell monolayer investigated with terahertz spectroscopy, Appl. Phys. Lett. 106 (2015), 253701, https://doi.org/10.1063/1.4922918.

[8] S.H. Lee, D. Lee, M.H. Choi, J.H. Son, M. Seo, Highly sensitive and selective detection of steroid hormones using terahertz molecule-specific sensors, Anal. Chem. 91 (2019) 6844–6849, https://doi.org/10.1021/acs.analchem.9b01066.

[9] M. Swithenbank, A.D. Burnett, C. Russell, L.H. Li, A.G. Davies, E.H. Linfield, J. E. Cunningham, C.D. Wood, On-chip terahertz-frequency measurements of liquids, Anal. Chem. 89 (2017) 7981–7987, https://doi.org/10.1021/acs.analchem.7b01235.

[10] K. Yang, X. Yang, X. Zhao, M.L. de la Chapelle, W. Fu, THz spectroscopy for a rapid and label-free cell viability assay in a microfluidic chip based on an optical clearing agent, Anal. Chem. 91 (2019) 785–791, https://doi.org/10.1021/acs.analchem.8b03665.

[11] A. Ahmadivand, B. Gerislioglu, P. Manickam, A. Kaushik, S. Bhansali, M. Nair, N. Pala, Rapid detection of infectious envelope proteins by magnetoplasmonic toroidal metasensors, ACS Sens. 2 (2017) 1359–1368, https://doi.org/10.1021/acssensors.7b00478.

[12] X. Zhao, M. Zhang, D. Wei, Y. Wang, S. Yan, M. Liu, X. Yang, K. Yang, H.L. Cui, W. Fu, Label-free sensing of the binding state of MUC1 peptide and anti-MUC1 aptamer solution in fluidic chip by terahertz spectroscopy, Biomed. Optic Express 8 (2017) 4427–4437, https://doi.org/10.1364/BOE.8.004427.

[13] W. Xu, L. Xie, J. Zhu, X. Xu, Z. Ye, C. Wang, Y. Ma, Y. Ying, Gold nanoparticle-based terahertz metamaterial sensors: mechanisms and applications, ACS Photonics 3 (2016) 2308–2314, https://doi.org/10.1021/acsphotonics.6b00463.

[14] D. Han, J. Li, W. Tan, CRISPR propels a smart hydrogel, Science 365 (2019) 754, https://doi.org/10.1126/science.aay4198.

[15] R. Liu, Y. Huang, Y. Ma, S. Jia, M. Gao, J. Li, H. Zhang, D. Xu, M. Wu, Y. Chen, Z. Zhu, C. Yang, Design and synthesis of target-responsive aptamer-cross-linked hydrogel for visual quantitative detection of ochratoxin A, ACS Appl. Mater. Interfaces 7 (2015) 6982–6990, https://doi.org/10.1021/acsami.5b01120.

[16] Z.T. Lin, Y. Li, J. Gu, H. Wang, Z. Zhu, X. Hong, Z. Zhang, Q. Lu, J. Qiu, X. Wang, J. Bao, T. Wu, A conductive nanowire-mesh biosensor for ultrasensitive detection of serum C-reactive protein in melanoma, Adv. Funct. Mater. 28 (2018), 1802482, https://doi.org/10.1002/adfm.201802482.

[17] S. Liu, W. Su, Y. Li, L. Zhang, X. Ding, Manufacturing of an electrochemical biosensing platform based on hybrid DNA hydrogel: taking lung cancer-specific miR-21 as an example, Biosens. Bioelectron. 103 (2018) 1–5, https://doi.org/10.1016/j.bios.2017.12.021.

[18] L. Xu, R. Wang, L.C. Kelso, Y. Ying, Y. Li, A target-responsive and size-dependent hydrogel aptasensor embedded with QD fluorescent reporters for rapid detection of avian influenza virus H5N1, Sensor. Actuator. B Chem. 234 (2016) 98–108, https://doi.org/10.1016/j.snb.2016.04.156.

[19] Y.J. Lee, S.A. Pruzinsky, P.V. Braun, Glucose-sensitive inverse opal hydrogels: analysis of optical diffraction response, Langmuir 20 (2004) 3096–3106, https://doi.org/10.1021/la035555x.

[20] D.A. Newnham, P.F. Taday, Pulsed terahertz attenuated total reflection spectroscopy, Appl. Spectrosc. 62 (2008) 394–398, https://doi.org/10.1366/000370208784046731.

[21] K. Shiraga, Y. Ogawa, T. Suzuki, N. Kondo, A. Irisawa, M. Imamura, Determination of the complex dielectric constant of an epithelial cell monolayer in the terahertz region, Appl. Phys. Lett. 102 (2013), 053702, https://doi.org/10.1063/1.4790392.

[22] K. Shiraga, Y. Ogawa, N. Kondo, A. Irisawa, M. Imamura, Evaluation of the hydration state of saccharides using terahertz time-domain attenuated total reflection spectroscopy, Food Chem. 140 (2013) 315–320, https://doi.org/10.1016/j.foodchem.2013.02.066.

[23] T. Elshaarani, H. Yu, L. Wang, A. Zain ul, R.S. Ullah, M. Haroon, R.U. Khan, S. Fahad, A. Khan, A. Nazir, M. Usman, K.U.R. Naveed, Synthesis of hydrogel-bearing phenylboronic acid moieties and their applications in glucose sensing and insulin delivery, J. Mater. Chem. B 6 (2018) 3831–3854, https://doi.org/10.1039/C7TB03332J.

[24] J.A. Morales-Hernández, A.K. Singh, S.J. Villanueva-Rodriguez, E. Castro-Camus, Hydration shells of carbohydrate polymers studied by calorimetry and terahertz spectroscopy, Food Chem. 291 (2019) 94–100, https://doi.org/10.1016/j.foodchem.2019.03.132.

[25] M. Mesch, C. Zhang, P.V. Braun, H. Giessen, Functionalized hydrogel on plasmonic nanoantennas for noninvasive glucose sensing, ACS Photonics 2 (2015) 475–480, https://doi.org/10.1021/acsphotonics.5b00004.

[26] T. Kajisa, T. Sakata, Glucose-responsive hydrogel electrode for biocompatible glucose transistor, Sci. Technol. Adv. Mater. 18 (2017) 26–33, https://doi.org/10.1080/14686996.2016.1257344.

[27] Q. Wang, M. Fu, Y. Guan, T.D. James, Y. Zhang, Mechanistic insights into the novel glucose-sensitive behavior of P(NIPAM-co-2-AAPBA), Sci. China Chem. 63 (2020) 377–385, https://doi.org/10.1007/s11426-019-9680-6.

[28] X. Yang, D. Wei, S. Yan, Y. Liu, S. Yu, M. Zhang, Z. Yang, X. Zhu, Q. Huang, H. L. Cui, W. Fu, Rapid and label-free detection and assessment of bacteria by terahertz time-domain spectroscopy, J. Biophot. 9 (2016) 1050–1058, https://doi.org/10.1002/jbio.201500270.

[29] M. Dautta, M. Alshetaiwi, J. Escobar, P. Tseng, Passive and wireless, implantable glucose sensing with phenylboronic acid hydrogel-interlayer RF resonators, Biosens. Bioelectron. 151 (2020), 112004, https://doi.org/10.1016/j.bios.2020.112004.

[30] Z. Zhang, P. Maturavongsadit, J. Shang, J. Yan, D. Li, Q. Wang, Q. Lin, A dielectric affinity glucose microsensor using hydrogel-functionalized coplanar electrodes, Microfluid. Nanofluidics 21 (2017) 93, https://doi.org/10.1007/s10404-017-1926-3.

[31] M. Elsherif, M.U. Hassan, A.K. Yetisen, H. Butt, Glucose sensing with phenylboronic acid functionalized hydrogel-based optical diffusers, ACS Nano 12 (2018) 2283–2291, https://doi.org/10.1021/acsnano.7b07082.